JCI insight

RESEARCH ARTICLE

β_1 Integrin regulates adult lung alveolar epithelial cell inflammation

Erin J. Plosa,[1] John T. Benjamin,[1] Jennifer M. Sucre,[1] Peter M. Gulleman,[1] Linda A. Gleaves,[2] Wei Han,[2] Seunghyi Kook,[1] Vasiliy V. Polosukhin,[2] Scott M. Haake,[3,4] Susan H. Guttentag,[1] Lisa R. Young,[5] Ambra Pozzi,[4,6,7] Timothy S. Blackwell,[2,4,8] and Roy Zent[4,6,8]

[1]Division of Neonatology, Department of Pediatrics, [2]Division of Allergy, Pulmonary, and Critical Care Medicine, Department of Medicine, and [3]Division of Hematology and Oncology, Department of Medicine, Vanderbilt University Medical Center, Nashville, Tennessee, USA. [4]Nashville Veterans Affairs Medical Center, Nashville, Tennessee, USA. [5]Division of Pulmonary Medicine, Department of Pediatrics, Children's Hospital of Philadelphia, Philadelphia, Pennsylvania, USA. [6]Division of Nephrology and Hypertension, Department of Medicine, [7]Department of Molecular Physiology and Biophysics, and [8]Department of Cell and Developmental Biology, Vanderbilt University Medical Center, Nashville, Tennessee, USA.

Integrins, the extracellular matrix receptors that facilitate cell adhesion and migration, are necessary for organ morphogenesis; however, their role in maintaining adult tissue homeostasis is poorly understood. To define the functional importance of β_1 integrin in adult mouse lung, we deleted it after completion of development in type 2 alveolar epithelial cells (AECs). Aged β_1 integrin–deficient mice exhibited chronic obstructive pulmonary disease–like (COPD-like) pathology characterized by emphysema, lymphoid aggregates, and increased macrophage infiltration. These histopathological abnormalities were preceded by β_1 integrin–deficient AEC dysfunction such as excessive ROS production and upregulation of NF-κB–dependent chemokines, including CCL2. Genetic deletion of the CCL2 receptor, *Ccr2*, in mice with β_1 integrin–deficient type 2 AECs impaired recruitment of monocyte-derived macrophages and resulted in accelerated inflammation and severe premature emphysematous destruction. The lungs exhibited reduced AEC efferocytosis and excessive numbers of inflamed type 2 AECs, demonstrating the requirement for recruited monocytes/macrophages in limiting lung injury and remodeling in the setting of a chronically inflamed epithelium. These studies support a critical role for β_1 integrin in alveolar homeostasis in the adult lung.

Introduction

Integrins are heterodimeric transmembrane receptors consisting of α and β subunits that bind extracellular matrix (ECM) components; propagate bidirectional signaling (1–5); and regulate critical processes such as adhesion, migration and proliferation that are required for the development of multicellular organisms (6–10). Of the 24 known α-β integrin heterodimers, 12 integrins contain the β_1 subunit. β_1 Integrins are present in epithelial cells, where they mediate cell adhesion to basement membranes and facilitate epithelial tissue organogenesis (9, 11–24). Compared with organ development, the function of integrins in maintaining tissue homeostasis is poorly defined.

Alveoli are complex structures composed of epithelial cells attached to a basement membrane juxtaposed to capillaries and stromal fibroblasts. Epithelial cells are either cuboidal type 2 alveolar epithelial cells (AECs) expressing high levels of surfactant protein C (SP-C) or very thin type 1 AECs in close apposition to capillaries. We previously reported that β_1 integrin regulates branching morphogenesis and alveolarization during lung development (22). Moreover, we showed that genetically deleting β_1 integrin in the developing alveolus results in dilated airspaces, thickened alveolar septa, type 2 AEC hyperplasia, and increased numbers of alveolar macrophages. Macrophage depletion rescued the alveolarization defect in these mice (22). These findings suggest that epithelial β_1 integrin dysfunction has deleterious consequences in lung epithelium through regulation of innate immunity. The mechanisms whereby these epithelial-macrophage interactions occur are uncertain, and, perhaps more importantly, the function of β_1 integrin in the adult lung is not established.

In this study, we deleted β_1 integrin in type 2 AECs after completion of lung development, which occurs by P28. At 2 years of age, the mice developed emphysematous changes in the lung parenchyma, as

Conflict of interest: The authors have declared that no conflict of interest exists.

Submitted: April 1, 2019
Accepted: December 12, 2019
Published: January 30, 2020.

Reference information: *JCI Insight*. 2020;5(2):e129259. https://doi.org/10.1172/jci.insight.129259.

well as lymphoid aggregates and increased macrophage accumulation, which are characteristic of patients with advanced chronic obstructive pulmonary disease (COPD). This condition was preceded by proliferation of inflamed AECs that exhibited abnormal cell-cell junctions and excessive inflammation. Reduction of monocytes and monocyte-derived macrophages caused rapid onset of emphysema in young mice, suggesting that these cells limit inflammation and injury by clearance of deranged type 2 AECs. Thus, we conclude that under physiological conditions, β_1 integrin plays a critical homeostatic role in lung epithelial cells by suppressing inflammatory signaling.

Results

Conditional β_1 integrin deletion in type 2 AECs results in emphysema and increased inflammation in aged mice. To test the importance of β_1 integrin deletion after development, we crossed integrin $\beta_1^{fl/fl}$ ($\beta1^{f/f}$) mice with a doxycycline-inducible (dox-inducible) Cre recombinase under control of the surfactant protein-C (SP-C) promoter (designated as $\beta1^{rtTA}$ mice). β_1 Integrin deletion was induced in type 2 AECs by addition of dox to drinking water from day P28, at the completion of lung development, until 2 months of age. Mice were sacrificed at 3 and 24 months of age. Lungs of 24-month-old $\beta1^{rtTA}$ mice exhibited emphysema and increased numbers of macrophages (Figure 1, A and B). Lung morphometry quantification by mean linear intercept demonstrated a 60% airspace enlargement in $\beta1^{rtTA}$ lungs compared with both $\beta1^{f/f}$ and $\beta1^{rtTA}$ mice that did not receive dox (Figure 1, C and D). Multiple lobes were sampled to minimize bias introduced by regional differences in alveolar size (25–27). There was evidence of bronchus-associated lymphoid tissue (BALT), which is characteristic of advanced COPD (arrows in Figure 1A, quantified in Figure 1E; and ref. 28). In addition to BALT lesions, histological examination revealed increased macrophages in $\beta1^{rtTA}$ lungs, identified by the pan-macrophage marker CD68 (Figure 1F), and an increase in bronchoalveolar lavage fluid (BALF) cell count ($1.8 \times 10^5 \pm 0.2 \times 10^5$ cells/mL from $\beta1^{rtTA}$ lungs compared with $0.8 \times 10^5 \pm 0.1 \times 10^5$ cells/ml from $\beta1^{f/f}$ lungs; Supplemental Figure 1A; supplemental material available online with this article; https://doi.org/10.1172/jci.insight.129259DS1).

Epithelial dysfunction precedes major morphological changes in $\beta1^{rtTA}$ mice. To determine the timing of the structural deficits in $\beta1^{rtTA}$ lungs relative to gene deletion, we performed histological examination of 3-month-old mice. We verified the efficiency of β_1 integrin deletion in the lungs of $\beta1^{rtTA}$ mice by immunohistochemistry and found it was removed in more than 90% of type 2 AECs (Figure 2, A and B). This finding was confirmed by immunoblotting of primary type 2 AEC lysates from $\beta1^{rtTA}$ and $\beta1^{f/f}$ mice (Figure 2C). Microscopic examination showed no difference in airspace size in 3-month-old $\beta1^{rtTA}$ mice (Figure 3, A and B). By crossing $\beta1^{rtTA}$ mice to mice expressing the mTmG reporter (allowing visualization of GFP^+ progeny derived from cells that had undergone Cre activation), we observed that $\beta1^{rtTA}$; mTmG mice exhibited GFP^+ type 1 AECs immediately adjacent to β_1-deficient type 2 AECs, suggesting β_1 integrin is not required for type 2–to–type 1 AEC differentiation during homeostasis in the adult lung (Supplemental Figure 1B). $\beta1^{rtTA}$ mice did exhibit mild intraseptal edema (arrows in Figure 3C), increased BALF protein (Supplemental Figure 2A), and increased BALF macrophages (Supplemental Figure 2B). Transmission electron microscopy (TEM) revealed intact cell-matrix interactions (arrows in Figure 3D) and defects in tight junctions between type 1 and type 2 AECs. Rather than the normal dark stranded seal demarcating tight junctions at the apical cell-cell junction, $\beta1^{rtTA}$ lungs had a deep cleft (Figure 3, D and E, with tight junctions marked by asterisks in E). Consistent with these tight junction abnormalities, $\beta1^{rtTA}$ mice had decreased claudin-3 protein levels in primary type 2 AEC lysates (Figure 3F) and decreased mRNA expression of *Claudin-4* but not *Claudin-18* as measured by quantitative RT-PCR (qPCR) of type 2 AECs (Figure 3G).

We next assessed whether there were abnormalities of type 2 AEC-ECM interactions by visualizing their adherence to the laminin-containing basement membrane. While the basal surface of type 2 AECs appeared to adhere normally to the basement membrane (Figure 4A), we noticed that there were more type 2 AECs in $\beta1^{rtTA}$ than $\beta1^{f/f}$ mice (Figure 4, B and C). The excess of type 2 AECs, evidenced by pro–SP-C–positive staining, was due to increased cellular proliferation that was identified by Ki-67 immunostaining (Figure 4, D and E). In contrast, no differences in the number of apoptotic type 2 AECs between $\beta1^{rtTA}$ and $\beta1^{f/f}$ lungs were observed, as demonstrated by dual $TUNEL^+$pro–$SP\text{-}C^+$ cells (Figure 4, F and G). Thus, deletion of β_1 integrin in AECs from 3-month-old adult mice caused subtle structural defects with abnormal tight junctions that likely allowed for paracellular fluid flux leak and type 2 AEC proliferation. Proliferation of type 2 AECs is a well-known feature of inflammatory lung diseases and a recognized consequence of lung injury (29–35); therefore, this finding suggests an ongoing injury-repair cycle.

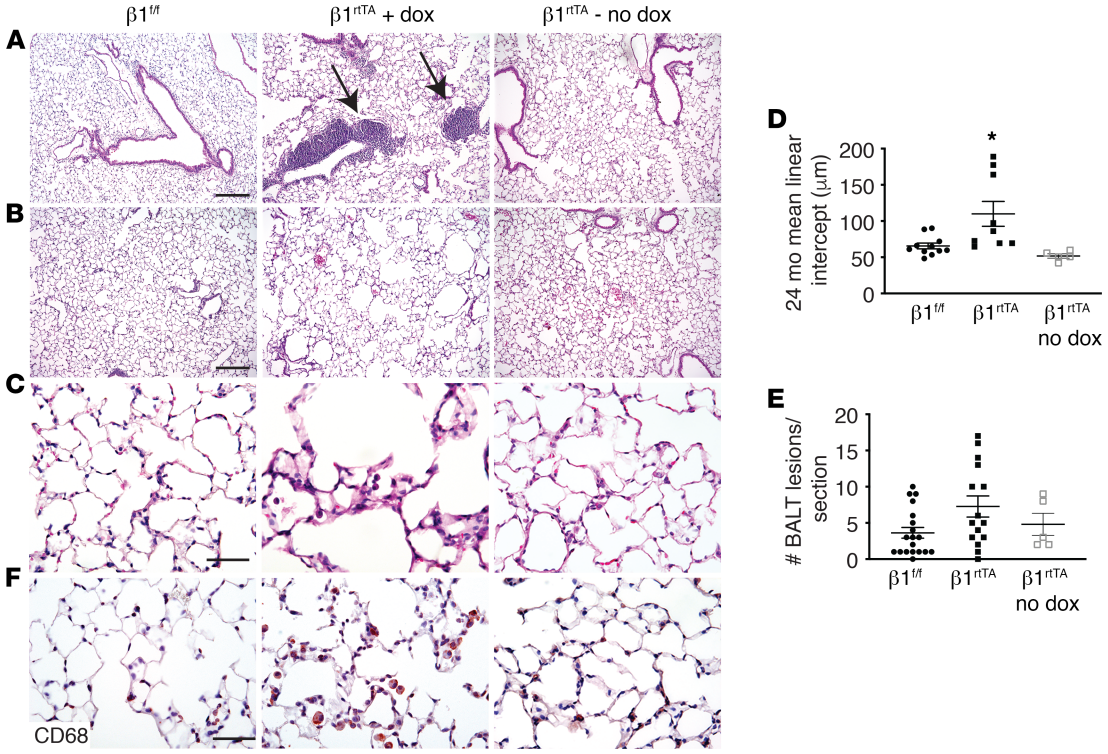

Figure 1. Deletion of β_1 integrin in type 2 AECs results in emphysema and increased inflammation in aged mice. (**A** and **B**) H&E-stained paraffin lung sections show marked airspace enlargement and increased number of BALT lesions in 24-month-old $\beta1^{rtTA}$ mice compared with age-matched $\beta1^{f/f}$ mice and 24-month-old dox-naive $\beta1^{rtTA}$ mice. Arrows indicate BALT lesions. (**C**) High-power images: Airspace enlargement is visible in $\beta1^{rtTA}$ lungs; quantification in **D** shows increased mean linear intercept in $\beta1^{rtTA}$ lungs (10 sections/mouse; $n = 11$ $\beta1^{f/f}$, $n = 9$ $\beta1^{rtTA}$ + dox mice, $n = 5$ $\beta1^{rtTA}$ – no dox mice). (**E**) Increased BALT lesions per lung section in $\beta1^{rtTA}$ mice. $n = 19$ $\beta1^{f/f}$, $n = 15$ $\beta1^{rtTA}$ + dox mice; $n = 5$ $\beta1^{rtTA}$ – no dox mice; $P = 0.0649$ by 1-way ANOVA. (**F**) $\beta1^{rtTA}$ lungs contain increased numbers of $CD68^+$ macrophages. Scale bars: 200 μm in **A** and **B**, 50 μm in **C** and **F**. $^*P < 0.05$ by 1-way ANOVA with Tukey's test for multiple comparison.

β_1 Integrin–deficient type 2 AECs induce increased efferocytosis. We next performed in-depth analysis of the inflammatory status of β1 integrin–deficient mice. When we examined aged $\beta1^{rtTA}$ mice, we noted that pro–SP-C staining often colocalized with CD68, suggesting that macrophages phagocytosed AECs in $\beta1^{rtTA}$ but not $\beta1^{f/f}$ lungs (Figure 5A). This observation is consistent with efferocytosis, a tightly regulated process by which phagocytic cells ingest diseased or dying cells, thereby minimizing inflammation in the microenvironment (36–39). To define the mechanisms whereby this occurred, we cultured primary type 2 AECs and measured secretion of CX3CL1, a "find me" chemokine that attracts phagocytes (40, 41). We also assessed the expression levels of *Cd47*, whose gene product is an inhibitory "don't eat me" signal, in freshly isolated primary type 2 AECs (41, 42). We found increased CX3CL1 production and reduced *Cd47* mRNA expression by $\beta1^{rtTA}$ type 2 AECs relative to type 2 AECs isolated from $\beta1^{f/f}$ mice (Figure 5, B and C). These findings support the conclusion that macrophage efferocytosis of β_1 integrin–deficient type 2 AECs is prominent in $\beta1^{rtTA}$ lungs.

Deleting CCL2-recruited monocytes/macrophages causes severe destruction of alveolar architecture in $\beta1^{rtTA}$ mice by decreasing AEC efferocytosis. Our histological examination of both aged and 3-month-old $\beta1^{rtTA}$ lungs suggested increased inflammation. Since $\beta1^{rtTA}$ lungs had increased macrophages, and β_1-null type 2 AECs exhibited markers of efferocytosis, we tested whether impairment of macrophage recruitment would disrupt homeostasis in 3-month-old $\beta1^{rtTA}$ mice. To target these recruited immune cell populations, we crossed $\beta1^{f/f}$ and $\beta1^{rtTA}$ mice to the *Ccr2*-null background. CCR2 is the receptor for CCL2, one of the primary monocyte chemokines in the lung. $CCR2^{-/-};\beta1^{rtTA}$ mice and their $CCR2^{-/-};\beta1^{f/f}$ littermate controls received dox from P28 until 2 months of age in the same manner as $\beta1^{f/f}$ and $\beta1^{rtTA}$ mice. In contrast to $\beta1^{rtTA}$ mice, 3-month-old $CCR2^{-/-};\beta1^{rtTA}$ mice exhibited dramatically enhanced lung pathology (Figure 6, A and B), with widespread emphysematous destruction; marked airspace enlargement, quantified by mean linear intercept (Figure 6C); increased inflammatory infiltrates (arrows in Figure 6B); and increased BALF cell counts (Figure 6D). $CCR2^{-/-};\beta1^{rtTA}$ mice exhibited a large number of $CD68^+$ macrophages (Figure 6, E and F) despite loss of CCL2 recruitment due to excessive proliferation of existing resident macrophages as verified by increased Ki-67 staining (Supplemental Figure 3, A–C).

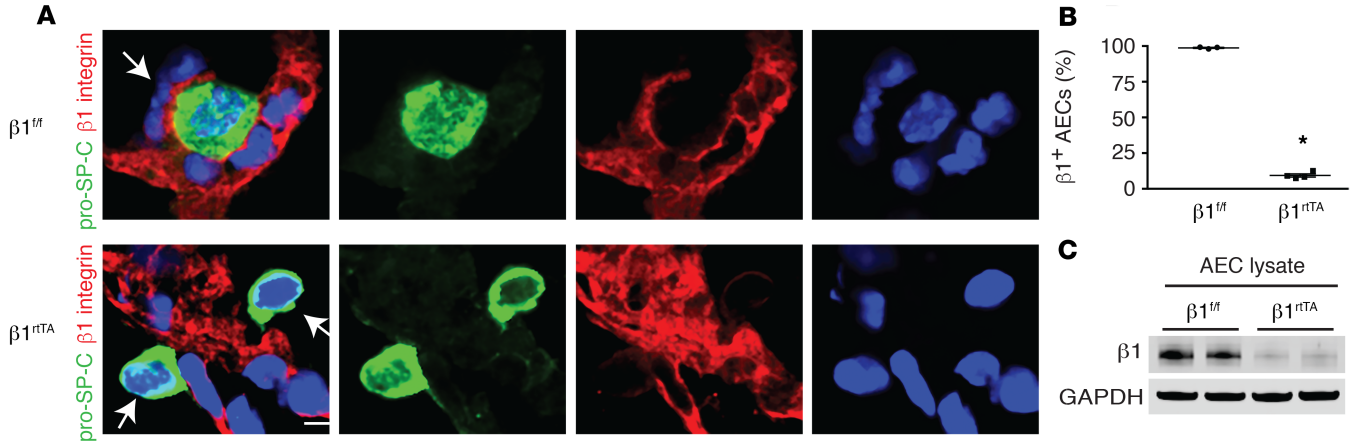

Figure 2. β_1 Integrin is deleted in type 2 AECs in $\beta1^{rtTA}$ lungs. (**A**) Immunostaining for pro–SP-C (green) and β_1 integrin (red) demonstrates type 2 AEC–specific deletion of β_1 integrin in 3-month-old $\beta1^{rtTA}$ lungs. Arrows indicate the presence/absence of β_1 integrin expression. Scale bar: 5 μm. (**B**) Type 2 AEC–specific deletion is represented as percentage of pro–SP-C$^+$ cells that express β_1 integrin. 100–120 type 2 AECs counted/mouse; n = 3 $\beta1^{f/f}$, n = 4 $\beta1^{rtTA}$ mice. (**C**) Representative Western blot for β_1 integrin on primary type 2 AEC lysate, normalized to GAPDH; representative of 3 separate experiments. *P < 0.05 by 2-tailed Student's t test.

A large increase in pro–SP-C$^+$ type 2 AECs accompanied the expanded immune cell population (Figure 6E, quantified in Figure 6G). Immunostaining for Ki-67 demonstrated that depletion of CCL2-driven monocytes/macrophages did not change the proliferation rate of AECs compared with $\beta1^{rtTA}$ mice (Supplemental Figure 3, D and E). These findings indicate that the increase in epithelial cell numbers in $\beta1^{rtTA}$ mice was due to impaired AEC removal rather than increased AEC proliferation. Despite numerous macrophages and an overabundance of type 2 AECs, there was almost no colocalization of CD68 and pro–SP-C in CCR2$^{-/-}$;$\beta1^{rtTA}$ mice (Figure 6H, quantified in Figure 6I), suggesting minimal efferocytosis in these mice. To directly test whether macrophages from CCR2$^{-/-}$;$\beta1^{rtTA}$ mice were defective in efferocytosis, we collected macrophages from bronchoalveolar lavage and exposed these cells to fluorescently labeled primary type 2 AECs from $\beta1^{rtTA}$ mice (Figure 6J). While macrophages from $\beta1^{rtTA}$ and $\beta1^{f/f}$ lungs briskly engulfed β_1-deficient AECs, macrophages from CCR2-deficient mice (both CCR2$^{-/-}$;$\beta1^{rtTA}$ and CCR2$^{-/-}$;$\beta1^{f/f}$) ingested far fewer labeled AECs, demonstrating that CCR2-deficient macrophages were less efficient efferocytosis agents. These data strongly suggest that the more severe phenotype in the CCR2$^{-/-}$;$\beta1^{f/f}$ mice is caused by their inability to remove deranged type 2 AECS and that the efferocytosis function of CCL2-recruited macrophages is to limit inflammation and mitigate lung damage in $\beta1^{rtTA}$ mice.

CD11b$^+$CD11c$^-$ monocytes/macrophages efferocytose type 2 AECs in $\beta1^{rtTA}$ mice. We next examined the immune cell population in the whole lung by flow cytometry. $\beta1^{rtTA}$ lungs contained increased CD45$^+$CD11b$^+$CD11c$^-$ immune cells, markers consistent with recently recruited monocyte–early macrophages (Figure 7A, gating strategy in Supplemental Figure 4; and refs. 43, 44). We identified this as a mixed population, as cells expressed the monocyte marker Ly6C, the macrophage marker CD64, or both (Figure 7B). Since the CD11b$^+$CD11c$^-$ immune cells were differentially enriched in $\beta1^{rtTA}$ mice, we collected this population by FACS, cytospinned the cells, and immunostained for pro–SP-C and CD68 to determine whether these cells contributed to the increased efferocytosis seen in $\beta1^{rtTA}$ mice. We found that 68% ± 4% of monocytes/macrophages collected from $\beta1^{rtTA}$ lungs contained pro–SP-C$^+$ material compared with 14% ± 2% of these cells from $\beta1^{f/f}$ lungs (Figure 7, C and D). To functionally phenotype these cells in $\beta1^{rtTA}$ mice, we collected media from cultured monocytes/macrophages and assayed for cytokine production by cytokine multiplex. The $\beta1^{rtTA}$ monocyte-macrophage population secreted only scant amounts of inflammatory cytokines/chemokines, equivalent to expression levels by cells from $\beta1^{f/f}$ mice (Supplemental Table 1). Taken together, these data demonstrate that CD11b$^+$CD11c$^-$ monocytes/macrophages are critical effector cells for efferocytosis but do not directly contribute to the inflammatory state of $\beta1^{rtTA}$ mice.

β1 Integrin regulates AEC inflammation. Our data thus far suggest that the β1 integrin–null cells provide an inflammatory stimulus resulting in monocyte-macrophage chemoattraction into the alveolus. These recruited cells function as efferocytotic agents but do not contribute to the inflammatory status of the lungs.

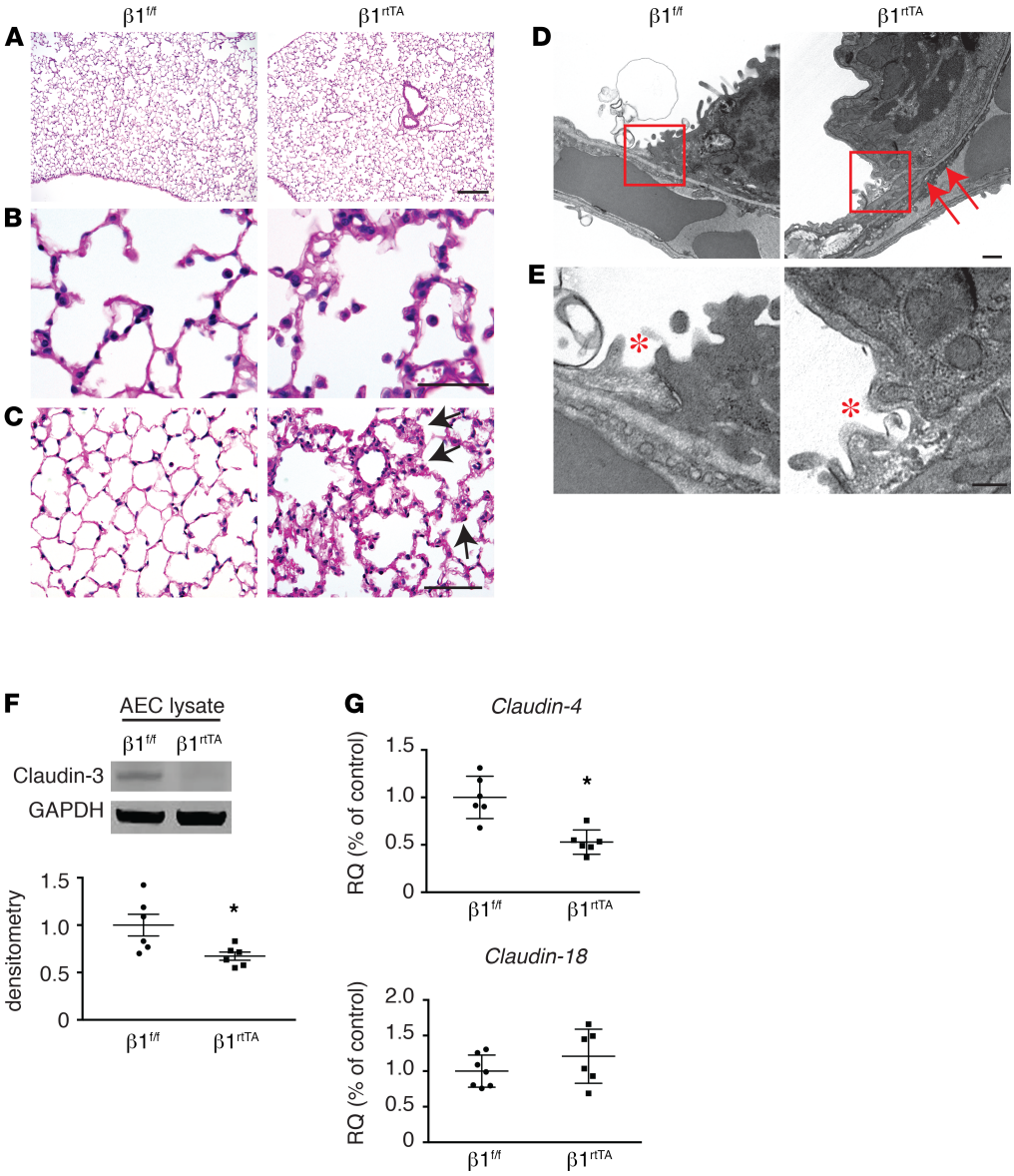

Figure 3. In the absence of aging, deletion of β_1 integrin in type 2 AECs minimally alters gross alveolar structure but results in epithelial dysfunction. (**A** and **B**) H&E-stained paraffin lung sections from 3-month-old $\beta1^{f/f}$ and $\beta1^{rtTA}$ mice demonstrate equal airspace size. (**C**) H&E-stained paraffin lung sections show increased intraseptal edema (arrows) in $\beta1^{rtTA}$ lungs. (**D** and insets in **E**) Transmission electron microscopic images of $\beta1^{f/f}$ and $\beta1^{rtTA}$ lungs show intact cell-matrix interactions (arrows in **D**), but clefts at the cell-cell junctions in $\beta1^{rtTA}$ lungs (junctions marked by asterisks in **E**). (**F**) Representative Western blot for claudin-3 on primary type 2 AEC lysate, with densitometry. *n* = 6 mice/group, normalized to GAPDH. (**G**) Gene expression for *Claudin-4* and *Claudin-18* by qPCR. *n* = 6 mice/group, normalized to GAPDH. RQ, relative quantitation. Scale bars: 200 μm in **A**, 25 μm in **B**, 50 μm in **C**, 500 nm in **D**, 250 nm in **E**. **P* < 0.05 by 2-tailed Student's *t* test. Images in **A**–**C** are representative of 6 mice/group.

Next, we tested whether β_1-deficient AECs drive the inflammatory phenotype in lungs of $\beta1^{rtTA}$ mice. Ten of 32 cytokines (31%), including mediators of macrophage chemotaxis and maturation, were significantly increased in the culture media of $\beta1^{rtTA}$ AECs compared with that of $\beta1^{f/f}$ AECs (Figure 8A and Supplemental Table 2). To define the consequence of increased AEC inflammatory signaling in the whole lung, we performed multiplex analysis on tissue lysates (Figure 8B and Supplemental Table 3). Multiple inflammatory mediators were increased in lungs of $\beta1^{rtTA}$ mice compared with $\beta1^{f/f}$ controls. Even further increases were seen in $CCR2^{-/-};\beta1^{rtTA}$, where inflamed β_1-deficient type 2 AECs remained unchecked by efferocytosis. Since many of the cytokines increased in $\beta1^{rtTA}$ and $CCR2^{-/-};\beta1^{rtTA}$ lungs were recognizable gene products of NF-κB signaling (including KC, IL-6, MIP-2, and G-CSF), we

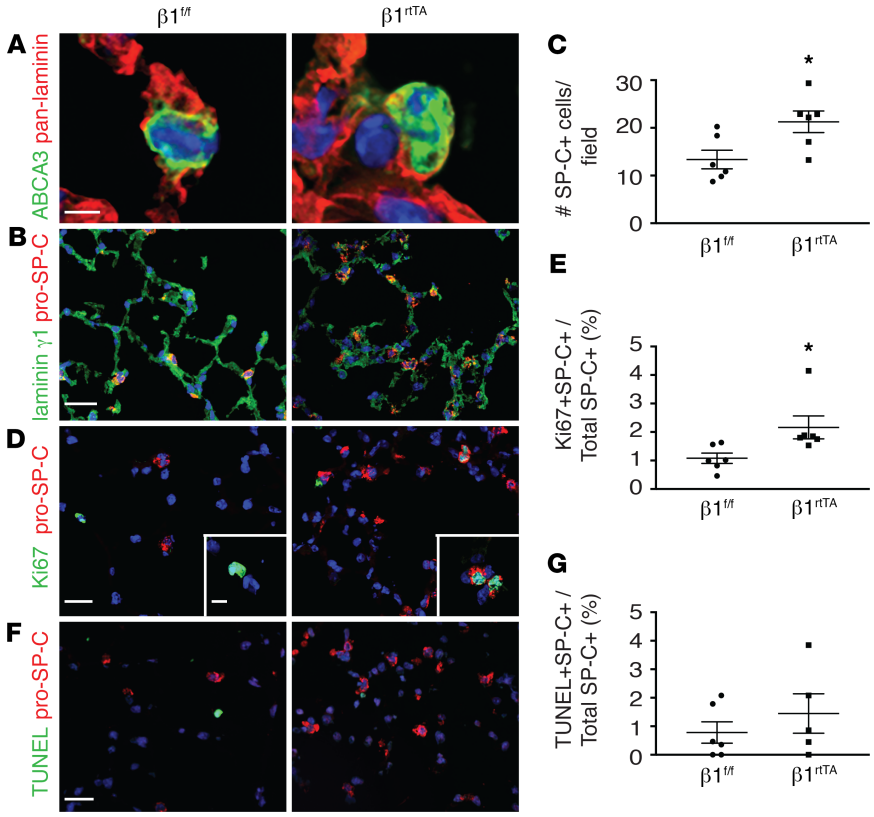

Figure 4. Loss of type 2 AEC β_1 integrin results in epithelial proliferation. (**A**) ABCA3$^+$ type 2 AECs (green) remain adherent to the basement membrane (laminin in red) in $\beta1^{rtTA}$ lungs. (**B**) Lung sections immunostained for type 2 AEC marker pro–SP-C (red) and laminin γ1 (green) show increased numbers of type 2 AECs in $\beta1^{rtTA}$ lungs, as quantified in **C**. 20 sections/mouse; n = 6 mice/group. (**D**) Lung sections immunostained for pro–SP-C (red) and the proliferation marker Ki-67 (green) show increased type 2 AEC proliferation in $\beta1^{rtTA}$ lungs, as quantified in **E**. 20 sections/mouse; n = 6 mice/group. (**F**) No difference in the number of apoptotic type 2 AECs in $\beta1^{rtTA}$ and $\beta1^{f/f}$ lungs, as identified by TUNEL and pro–SP-C costained type 2 AECs, as quantified in **G**. n = 6 $\beta1^{f/f}$, n = 5 $\beta1^{rtTA}$ mice. Scale bars: 5 μm in **A**; 50 m in **B**, **D** (10 μm for insets), and **F**. *P < 0.05 by 2-tailed Student's t test.

performed immunohistochemistry for activated NF-κB in β_1 integrin–deficient AECs (Figure 8, C and D). Immunofluorescence staining for phospho-p65 (S276), a well-recognized marker of NF-κB activation (45), revealed numerous phospho-p65$^+$pro–SP-C$^+$ type 2 AECs in lungs from $\beta1^{rtTA}$ mice and CCR2$^{-/-}$;$\beta1^{rtTA}$ mice. Other cell types, in addition to type 2 AECs, exhibited NF-κB activation in $\beta1^{rtTA}$ and CCR2$^{-/-}$;$\beta1^{rtTA}$ lungs. These findings indicate that β_1 integrin deficiency results in a pervasive inflammatory environment in the distal lung with contributions from retained β_1-deficient type 2 AECs.

β_1-Deficient AEC inflammatory mediators are produced as a consequence of ROS generation. Since the generation of ROS has been linked to NF-κB–dependent cytokine expression in epithelial cells and β_1-containing integrins have been shown to modulate ROS signaling (46–50), we measured ROS production in cultured type 2 AECs. We found that $\beta1^{rtTA}$ type 2 AECs produced more superoxide (O_2^-) and hydrogen peroxide (H_2O_2) than $\beta1^{f/f}$ cells (Figure 9, A and B); however, no differences in mitochondria-derived ROS were detected (Figure 9C). Given the increase in O_2^- generation, we investigated whether the NADPH oxidase (NOX) system was upregulated in cells from $\beta1^{rtTA}$ mice. Of the 5 major NADPH isoforms in the lung epithelium, *Duox1* expression was markedly increased in freshly isolated β_1–integrin deficient primary type 2 AECs, but there was no significant difference in expression of the NOX isoforms *Duox2*, *Nox1*, *Nox2*, or *Nox4* between β_1 integrin–deficient and control cells (Figure 9D).

To define whether ROS production stimulated NF-κB–dependent cytokine expression, we measured levels of CCL2, a known downstream cytokine product of NF-κB activation (51–53). We treated type 2 AECs isolated from $\beta1^{rtTA}$ and $\beta1^{f/f}$ mice with a superoxide dismutase mimetic (TEMPOL) or a pan-NOX inhibitor (DPI) and measured CCL2 concentration in the media by ELISA. Both TEMPOL and DPI

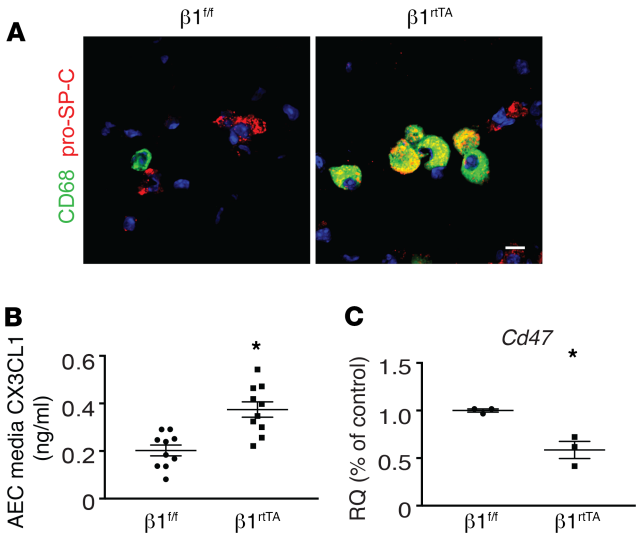

Figure 5. β1^{rtTA} mice have increased efferocytosis of type 2 AECs. (**A**) Aged 24-month-old β1^{rtTA} lungs exhibit increased colocalization of pro–SP-C (red) and CD68 (green), indicative of increased efferocytosis of type 2 AECs by macrophages. Scale bar: 10 μm. Representative of 3 mice/group. (**B**) Increased CX3CL1 by ELISA in media collected from primary β1^{rtTA} type 2 AECs after 24 hours in culture. *n* = 10 mice/group. (**C**) Decreased gene expression of *CD47* in freshly isolated primary type 2 AECs isolated from β1^{rtTA} mice. *n* = 3 mice/group. *$P < 0.05$ by 2-tailed Student's *t* test.

treatment decreased CCL2 secretion by β1^{rtTA} type 2 AECs (Figure 9, E and F). Although a specific Duox1 inhibitor is not available, we narrowed down the NOX subunits potentially regulated by β_1 integrin using the NOX1/4 inhibitor GKT137831 (Figure 9G). In contrast to the pan-NOX inhibitor DPI, treatment with GKT137831 did not reduce CCL2 secretion from β1^{rtTA} type 2 AECs, implicating NOX2, Duox1, and/or Duox2 as the source of increased ROS in β1^{rtTA} mice. As *Duox1* was the only NOX isoform with increased expression, these data suggest that β_1 integrin regulates ROS production through this isoform in AECs.

To test whether ROS-dependent CCL2 production by β1^{rtTA} type 2 AECs was in part responsible for increased macrophage infiltration in β1^{rtTA} mice, we performed chemotaxis assays using WT macrophages collected by bronchoalveolar lavage and conditioned media from cultured type 2 AECs from β1$^{f/f}$ and β1^{rtTA} mice. Macrophage migration toward media from β1^{rtTA} type 2 AECs was greatly enhanced compared with media from control cells, and this increase was completely abrogated by treatment with DPI or neutralizing antibodies to CCL2 (Figure 9H). These findings support the conclusion that β1^{rtTA} type 2 AECs have persistent ROS production that contributes to CCL2 secretion that induces macrophage migration into the airspaces of β1^{rtTA} mice.

Discussion

While numerous studies have defined the critical role of integrins in organ morphogenesis, few have examined their role in tissue homeostasis in adults. In the setting of development, phenotype severity is highly correlated with timing of integrin deletion after conception and is primarily ascribed to defects in cell adhesion and migration. In this study, we defined the role of β_1 integrin in the structurally stable, fully formed alveolus of the lung, where epithelial cells undergo slow turnover and are tightly bound to the basement membrane. We show that deleting β_1 integrin in AECs under these circumstances results in emphysema, a condition characterized by destruction/loss of gas exchange units and chronic inflammation. Surprisingly, there were no adhesion defects in the AECs in our model; however, these cells were highly inflamed, with excessive ROS production that caused increased NF-κB–dependent cytokine production. Thus, β_1 integrin in alveolar epithelial cells has an antiinflammatory role and is required for alveolar homeostasis in the lung.

Our studies provide direct evidence that mice with a targeted deletion of β_1 integrin in type 2 AECs develop aging-related, spontaneous emphysema as quantified by mean linear intercept. This method easily captures one component of the emphysematous phenotype, enlargement of airspaces. Although we did not perform stereological analysis to address alveolar number specifically, we took precautions

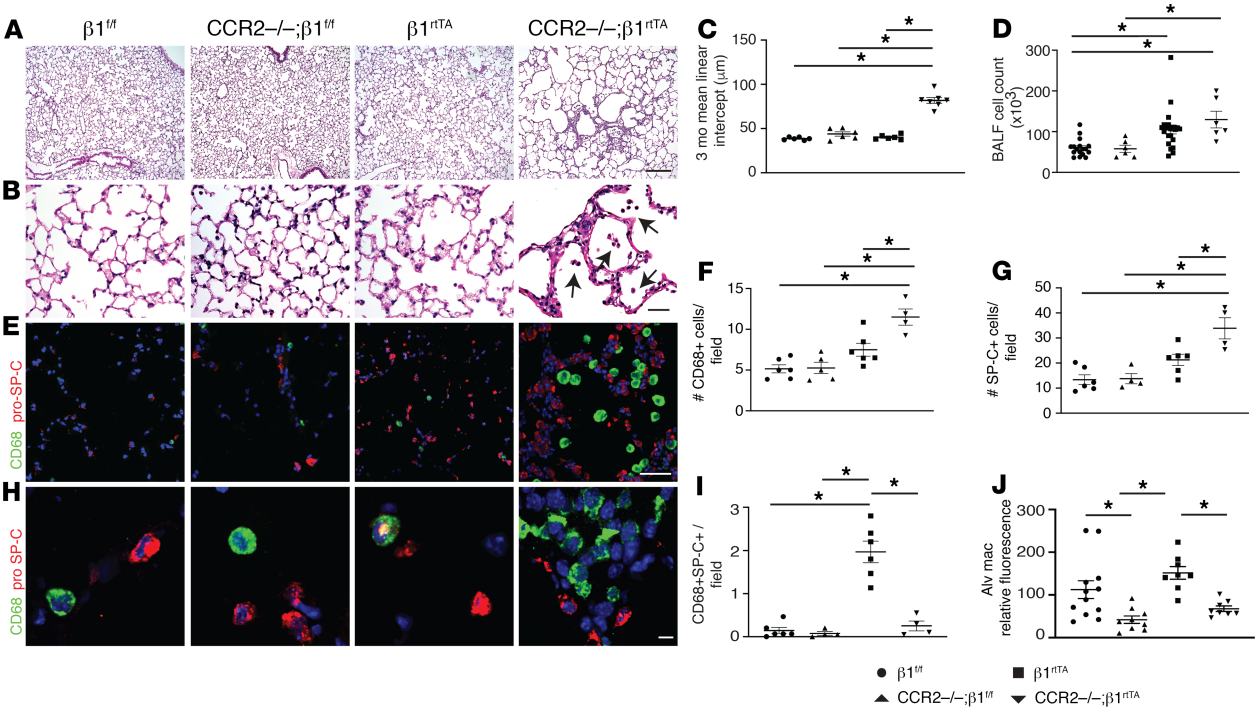

Figure 6. Recruited monocytes/macrophages maintain structural homeostasis in $\beta1^{rtTA}$ mice through efferocytosis. (**A** and **B**) $CCR2^{-/-};\beta1^{rtTA}$ lungs show severe remodeling and increased inflammatory infiltrate (arrows) in low-power (**A**) and high-power (**B**) images of H&E-stained sections. (**C**) Increased mean linear intercept in 3-month-old $CCR2^{-/-};\beta1^{rtTA}$ lungs. 6–10 sections/mouse; n = 6 $\beta1^{f/f}$, n = 6 $CCR2^{-/-};\beta1^{f/f}$, n = 6 $\beta1^{rtTA}$, n = 7 $CCR2^{-/-};\beta1^{rtTA}$ mice/group). (**D**) Increased BALF cell counts in $CCR2^{-/-};\beta1^{rtTA}$ mice. n = 17 $\beta1^{f/f}$; n = 6 $CCR2^{-/-};\beta1^{f/f}$, n = 21 $\beta1^{rtTA}$, n = 6 $CCR2^{-/-};\beta1^{rtTA}$ mice/group). (**E**) Immunostaining for CD68 (green) and pro–SP-C (red) demonstrates increased macrophages and type 2 AECs in $CCR2^{-/-};\beta1^{rtTA}$ lungs. (**F** and **G**) Quantification for numbers of $CD68^+$ (**F**) and pro–$SP\text{-}C^+$ cells/field (**G**). 20 sections/mouse; n = 4–6 mice/group. (**H** and **I**) Immunostaining demonstrates minimal colocalization of $CD68^+$ and pro–$SP\text{-}C^+$ cells in $CCR2^{-/-};\beta1^{f/f}$ and $CCR2^{-/-}$; $\beta1^{rtTA}$ lungs, whereas abundant colocalization was present in $\beta1^{rtTA}$ lungs. 20 sections/mouse; n = 4–6 mice/group. (**J**) Quantification of alveolar macrophage (Alv mac) efferocytosis of fluorescently labeled primary type 2 AECs. n = 8–12 mice/group. Scale bar: 200 μm in **A**, 50 μm in **B** and **E**, 5 μm in **H**. *$P < 0.05$ by ordinary 1-way ANOVA with secondary analysis by Tukey's test for multiple comparisons as indicated.

in our studies to minimize bias in our 2D morphological measurements from sampling (25–27). Loss of β_1 integrin in AECs stimulates ROS production and NF-κB signaling, and subsequently released inflammatory mediators recruit and activate a mixed population of monocytes/macrophages that efferocytose the β_1-deficient AECs. One possible mechanism for the development of emphysema is that macrophages mediate lung destruction via altered protease/antiprotease balance (54–56). These observations are consistent with studies demonstrating a role for excessive ROS and NF-κB activation as initiators of macrophage accumulation and subsequent alveolar injury, resulting in emphysema (57–59). In addition, epithelial apoptosis in combination with ineffective efferocytosis could contribute to the development of emphysema. Both epithelial and endothelial apoptosis can contribute to emphysema independent of inflammation (60–62). Consistent with these potential explanations for development of emphysema in our model, blocking efferocytosis has been shown to potentiate alveolar destruction in murine models of elastase-induced emphysema associated with increased MMP2 and -12 expression (63). It is unclear whether loss of efferocytosis with its antiinflammatory effects or the retention of inflamed β_1-deficient AECs causes emphysema. However, our data indicating that there is no phenotypical difference in the efferocytosing monocytes/macrophages suggest that retained β_1-deficient AECs are the primary driver of emphysema in $\beta1^{rtTA}$ mice. Our data also confirmed and extended studies that indirectly implicated β_1-containing integrins in the pathogenesis of emphysema. Mice with impaired fucosylation exhibit an emphysematous lung phenotype, and fucosylation is required for normal $\alpha_3\beta_1$ integrin–dependent migration and signaling, suggesting that the phenotype is due to impaired$\alpha_3\beta_1$integrin function (64, 65). Similarly, fibulin $5^{-/-}$ mice have enlarged airspaces at birth that progressively dilate into adulthood (66). Fibulin 5 is a ligand for $\alpha_v\beta_3$-, $\alpha_v\beta_5$, and $\alpha_9\beta_1$ integrins, participates in outside-in integrin signaling, and is crucial for proper assembly of elastic fibers (66, 67).

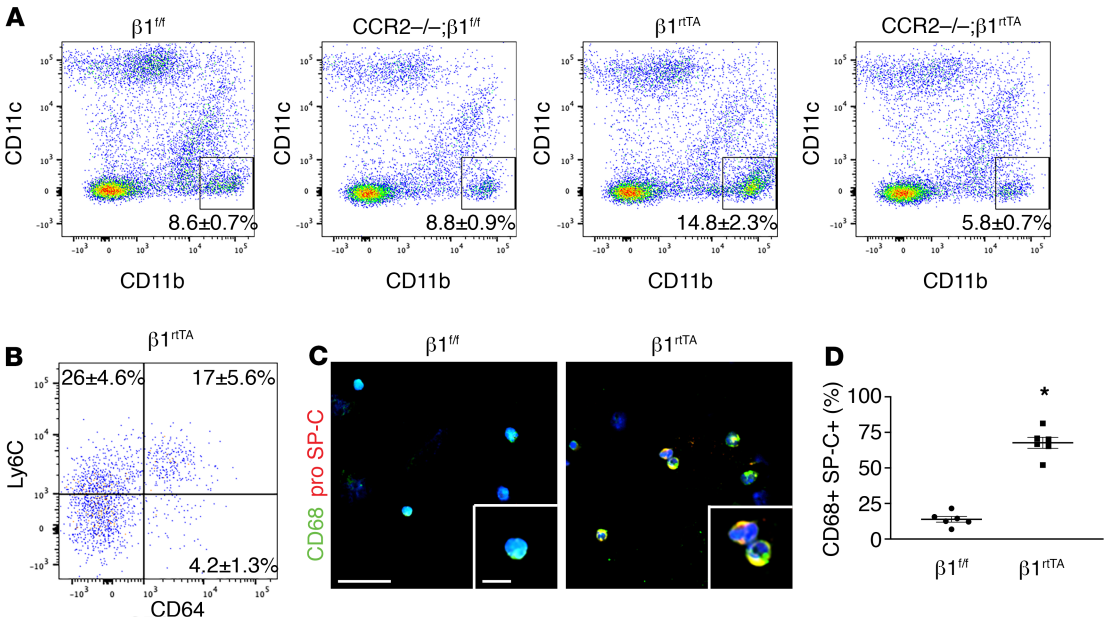

Figure 7. CD11b$^+$CD11c$^-$ monocytes/macrophages efferocytose type 2 AECs in β1^{rtTA} mice. (**A**) β1^{rtTA} lungs contain increased CD45$^+$CD11b$^+$CD11c$^-$ monocytes/macrophages by flow cytometry. n = 7 β1$^{f/f}$, n = 4 CCR2$^{-/-}$;β1$^{f/f}$, n = 6 β1^{rtTA}, and n = 7 CCR2$^{-/-}$;β1^{rtTA} mice. (**B**) CD45$^+$CD11b$^+$CD11c$^-$ population consists of cells that are both Ly6C$^+$ and CD64$^+$ in β1^{rtTA} lungs. n = 6 β1^{rtTA} mice. (**C**) Immunostained cytospins from CD45$^+$CD11b$^+$CD11c$^-$ monocytes/macrophages show increased numbers of CD68$^+$pro-SP-C$^+$ cells in β1^{rtTA} lungs, as quantified in **D**. n = 6 mice/group. Scale bar: 40 μm in **C**, 10 μm for inset. *P < 0.05 by 2-tailed Student's t test.

We show that the inflammatory phenotype of β_1 integrin–deficient AECs, as manifested by increased NF-κB signaling and cytokine production, is mediated at least in part by excessive ROS production. While this phenomenon is well documented in multiple other cell types (68–70), the mechanisms whereby integrins regulate ROS production are poorly understood. Our studies implicate β_1 integrin as a critical negative regulator of the NOX isoform *Duox1* in AECs. Previous studies reported that β_1 integrin negatively regulates ROS production through NOX2 in chondrocytes and kidney mesangial cells (46, 47, 71, 72). Thus, integrins play a critical role in regulating ROS production in multiple cell types; however, the mechanisms appear to be cell type specific.

One of the most interesting observations in our study was that genetic depletion of CCR2, which blocks CCL2-mediated recruitment of monocyte-derived macrophages, exacerbates alveolar remodeling in adult β_1–deficient mice. This contrasts with our previous observation that chemical depletion of macrophages using intranasal instillation of clodronate during lung development rescues alveolarization defects (22). These findings expose differential functions of macrophage subtypes and their potentially paradoxical roles in the adult versus developing lung. In development, fetal lung macrophages are essential for normal lung morphogenesis. They actively clear mesenchymal cells through phagocytosis during sacculation, and their response to inflammatory stimuli regulates airway branching through modulation of developmental signals (36–39, 73–75). During homeostasis, macrophages are required for regulation of inflammatory signaling, host defense, and wound healing (76, 77). The majority of efferocytosis activity following injury is accomplished by macrophages, but more recent data suggest that monocytes significantly contribute to efferocytosis and antigen presentation in the presence of apoptotic cells (78). Although monocytes and macrophages efferocytose dying cells during acute injury, their role in chronic inflammation is less well defined (78, 79). In our model, deranged type 2 AECs are efferocytosed by the CD11b$^+$CD11c$^-$ monocyte/macrophage population. This is likely a mix of newly recruited monocytes and monocytes transitioning into macrophages. In β1^{rtTA} mice, homeostatic compensation fails with loss of CCL2-driven monocyte-macrophage recruitment, resulting in an escalation of inflammation associated with diminished efferocytosis. Although determining why CCL2-recruited monocytes/macrophages are necessary for efficient efferocytosis of type 2 AECs will require further study, this finding could have direct implications for human lung diseases, including COPD, in which ineffective efferocytosis has been suggested to be a contributor to pathogenesis (80–86).

Aside from regulating inflammation, β_1 integrin is required for other critical cellular processes in type 2 AECs, including maintenance of tight junctions and control of proliferation. Microscopic examination of

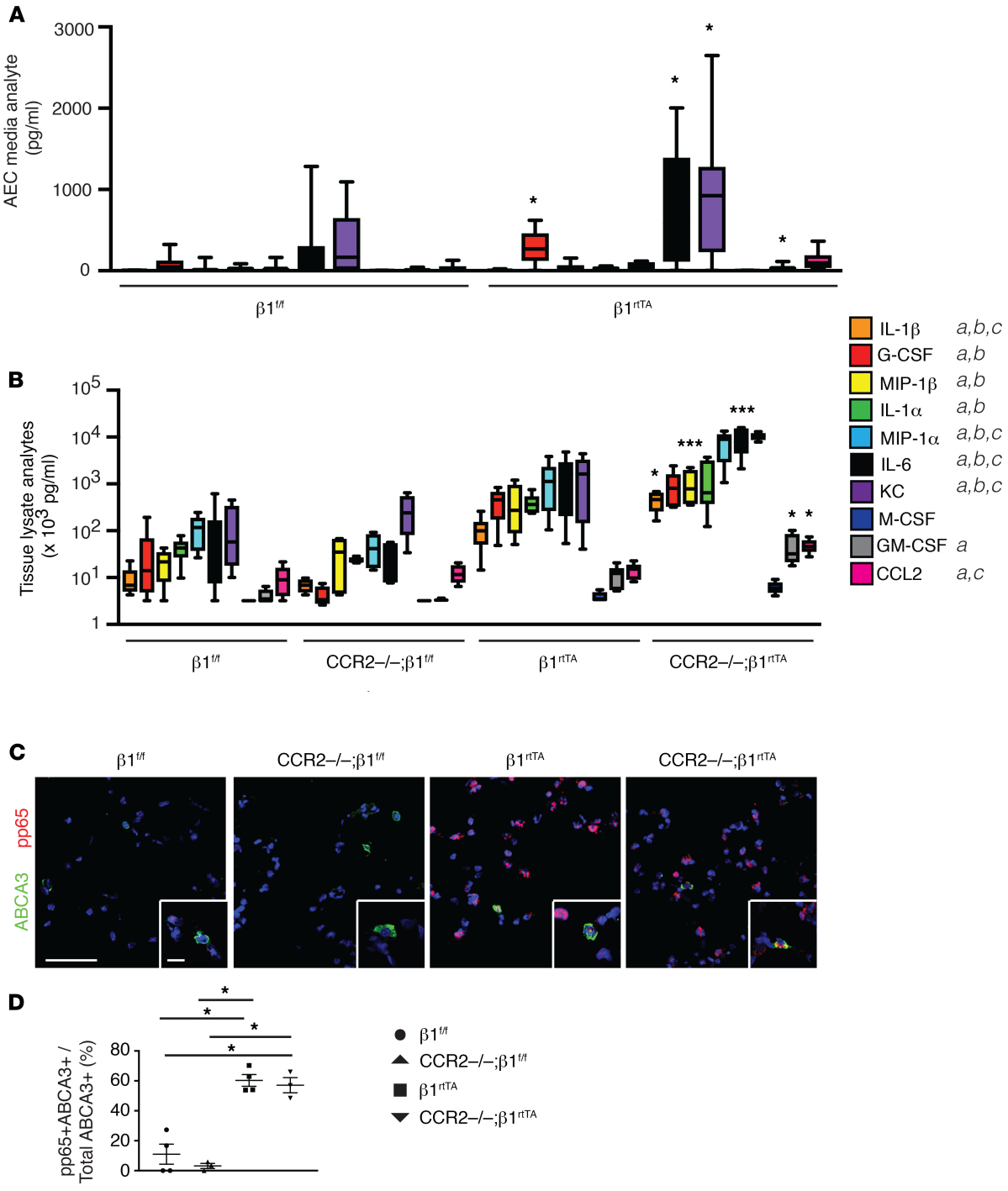

Figure 8. Loss of β_1 integrin results in widespread lung inflammation. (**A**) Increased proinflammatory cytokines in media collected from $\beta1^{rtTA}$ type 2 AECs compared with $\beta1^{f/f}$ type 2 AECs. *n* = 11–12 mice/group. (**B**) $\beta1^{rtTA}$ and $CCR2^{-/-};\beta1^{rtTA}$ lungs exhibit increased proinflammatory cytokines in whole lung tissue lysate by cytokine multiplex assay. *n* = 4–6 mice/group. (**C**) Immunostaining for phospho-p65 (red) and the type 2 AEC marker ABCA3 (green) demonstrates increased NF-κB activation in type 2 AECs and throughout the tissue in $\beta1^{rtTA}$ and $CCR2^{-/-};\beta1^{rtTA}$ lungs, as quantified in **D**. Fewer than 10 sections/mouse; *n* = 4 mice/group. Scale bars: 50 μm in **C**, 10 μm for insets. *$P < 0.05$ by 1-way ANOVA with secondary analysis by Tukey's test for multiple comparisons. *a*: $\beta1^{f/f}$ vs. $CCR2^{-/-};\beta1^{rtTA}$, *b*: $CCR2^{-/-};\beta1^{f/f}$ vs. $CCR2^{-/-};\beta1^{rtTA}$, *c*: $\beta1^{rtTA}$ vs. $CCR2^{-/-};\beta1^{rtTA}$.

$\beta1^{rtTA}$ mice revealed abnormal tight junctions associated with decreased *Claudin-3* and *Claudin-4* expression. Consistent with this observation, proximal kidney tubule cells with β_1 integrin deletion exhibit altered *Claudin-2* expression (87). Our epithelial β_1–null mice also share many phenotypic similarities with claudin-deficient mice. Unchallenged claudin-4–deficient mice have normal lung histology but exhibit significantly

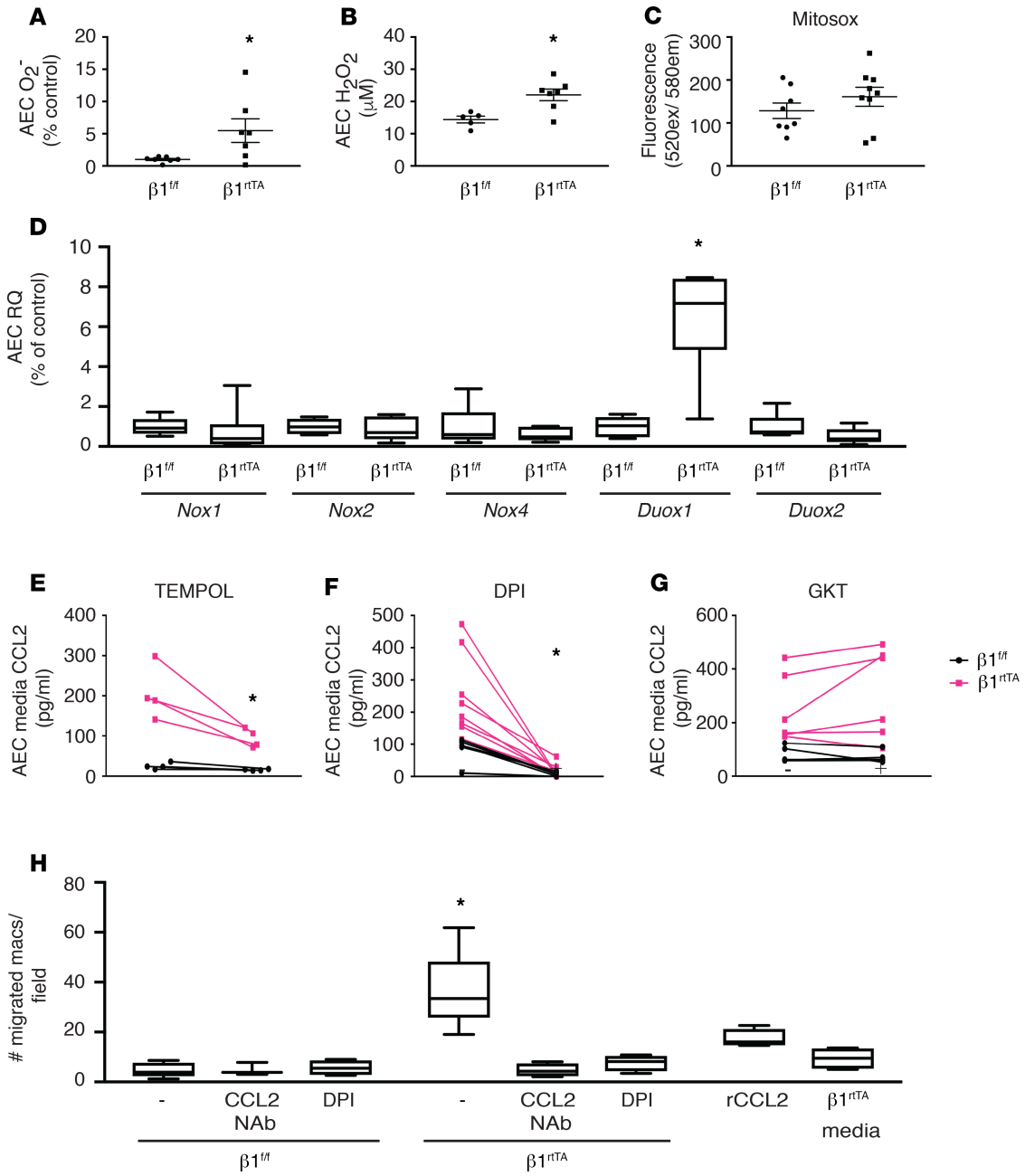

Figure 9. β_1-Deficient AECs generate excess inflammatory mediators via ROS production. (**A** and **B**) Primary $\beta1^{rtTA}$ type 2 AECs produce increased superoxide and H_2O_2 by LumiMax assay (**A**; n = 7 mice/group) and Amplex Red assay (**B**; n = 5 $\beta1^{f/f}$, n = 7 $\beta1^{rtTA}$ mice), respectively. (**C**) No difference in mitochondrial ROS production in $\beta1^{f/f}$ and $\beta1^{rtTA}$ type 2 AECs by MitoSOX assay. n = 8–9 mice/group. ex, excitation; em, emission. (**D**) Increased gene expression of *Duox1* in primary type 2 AECs isolated from $\beta1^{rtTA}$ mice. n = 6 mice/group. (**E**) TEMPOL treatment decreases CCL2 secretion by primary type 2 AECs isolated from $\beta1^{rtTA}$ mice. 2 mM; n = 4 mice/group). (**F**) DPI treatment decreases CCL2 secretion by primary type 2 AECs isolated from $\beta1^{rtTA}$ mice. 10 μM; n = 7 $\beta1^{f/f}$, n = 8 $\beta1^{rtTA}$ mice. (**G**) CCL2 secretion is not different between $\beta1^{f/f}$ and $\beta1^{rtTA}$ type 2 AECs after treatment with the NOX1/4 inhibitor GKT137831. 10 μM; n = 5 $\beta1^{f/f}$, n = 5 $\beta1^{rtTA}$ mice. (**H**) Macrophage migration in response to $\beta1^{rtTA}$ type 2 AEC media is decreased by treatment with CCL2-neutralizing antibody (NAb) and DPI. n = 4–8 mice/group. *P < 0.05 by 2-tailed Student's t test. CCR2, recombinant CCR2.

increased BALF cell counts with hyperoxia exposure and increased CCL2 signaling with mechanical ventilation (88). In addition, claudin-18–null mice develop AEC hyperplasia and macrophage accumulation over time (89–91). Although a causal relationship between β_1 integrin and claudins has not been described, previous in vitro studies demonstrated that ROS can disrupt tight junctions (92–94), suggesting that β_1 integrin–mediated ROS could regulate tight junctions via effects on claudin expression. Another phenotype identified in $\beta1^{rtTA}$ mice is AEC proliferation. Developmental deletion of β_1 integrin decreases epithelial

proliferation in the kidney, mammary, and submandibular glands (11, 15, 19, 21, 22), whereas increased epithelial proliferation has been reported when β_1 integrin was deleted in the intestine or skin (14, 17). The mechanisms whereby β_1 integrin regulates cell number/density in fully formed organs is unknown; however, this could also be ROS mediated, since multiple investigations have shown that ROS can stimulate cell proliferation.

In conclusion, this study shows that loss of β_1 integrin in type 2 AECs promotes persistent lung inflammation and emphysematous remodeling, which is mitigated by efferocytosis of inflamed AECs by $CD11b^+CD11c^-$ monocytes/macrophages. Thus, regulation of inflammation is the major function of β_1 integrin in alveolar homeostasis in the lung.

Methods

Mice. For timed deletion of β_1 integrin, we crossed transgenic mice with inducible Cre recombinase expression by the dox-inducible reverse tetracycline transactivator under control of the SP-C promoter (SP-C rtTA;Tet-O-Cre) with integrin $\beta_1^{fl/fl}$ mice (95, 96). Postdevelopmental type 2 AEC deletion was induced on P28 in these triple transgenic SP-C rtTA;Tet-O-Cre; $\beta1^{f/f}$ mice (called $\beta1^{rtTA}$ mice) using dox in drinking water (2 g/L × 4 weeks). Control littermate $\beta1^{f/f}$ mice received identical dox treatment. To test the role of β_1 integrin in epithelial differentiation during alveolar homeostasis, we crossed $\beta1^{rtTA}$ mice to the mTmG Cre recombinase reporter. To test the role of CCL2-recruited monocytes/macrophages in β1 integrin–regulated alveolar homeostasis, we crossed $\beta1^{rtTA}$ and $\beta1^{f/f}$ mice onto a homozygous null background for *Ccr2*, the CCL2 receptor. The resulting transgenic $CCR2^{-/-}$;SP-C rtTA;Tet-O-Cre;$\beta1^{f/f}$ mice (termed $CCR2^{-/-}$;$\beta1^{rtTA}$ mice) and control littermate $CCR2^{-/-}$;$\beta1^{f/f}$ mice, received identical dox treatment on P28 to induce β_1 integrin deletion. Integrin $\beta1^{f/f}$ mice were a gift from Elaine Fuchs (Howard Hughes Medical Institute, The Rockefeller University, New York, New York, USA). SP-C rtTA, Tet-O-Cre, *Ccr2* homozygous null, and mTmG Cre recombinase reporter mice were purchased from the Jackson Laboratory. All mice were on a C57BL/6 background.

Histology and morphological analysis. Lungs from $\beta1^{rtTA}$, $\beta1^{f/f}$, $CCR2^{-/-}$;$\beta1^{rtTA}$; and $CCR2^{-/-}$;$\beta1^{f/f}$ mice were harvested for histological examination. Mice were sacrificed, right ventricle flushed with PBS, and lung inflation fixed at 25 cm with 10% formalin for more than 24 hours prior to paraffin embedding and sectioning. Multiple lobes were sectioned to reduce bias in morphological analysis generated from regional differences in alveolar size (25–27). Mean linear intercept was calculated from images obtained using a Keyence BZ-X710 inverted fluorescence phase contrast microscope with ×40 objective for 6–10 nonoverlapping sections per mouse. For immunohistochemistry stains, paraffin sections were deparaffinized, antigen retrieved, blocked, and incubated with the indicated primary antibody, followed by colorimetric detection by Vector Red (Vector Laboratories). Stained paraffin sections were imaged using a Keyence BZ-X710 inverted fluorescence phase contrast microscope with ×20 objective lens (low-power images) or an Olympus BX41 with ×60 objective lens (high-power images). Immunofluorescence staining was performed on frozen lung sections that were inflation fixed with 2:1 PBS/O.C.T. mixture (Tissue-Tek), embedded, and sectioned at 8-μm thickness. Slides were subsequently fixed with 4% paraformaldehyde, permeabilized with 0.1% Triton-X, blocked with 5% donkey serum, incubated in primary antibody overnight at 4°C, incubated in secondary antibody for 2 hours at room temperature, incubated with DAPI nuclear stain (Vector Laboratories), mounted with ProLong Gold (Thermo Fisher Scientific), and imaged using a Nikon Spinning Disk TiE inverted fluorescence confocal microscope attached to an Andor DU-897 EMCCD camera (×20 or ×60 objective). The following primary antibodies were used: anti–pro–SP-C (Abcam ab90716), rabbit anti-CD68 (Abcam ab125212), rat anti-CD68 (Abcam ab53444), anti–β_1 integrin (Millipore MAB1997), anti–laminin γ1 (Novus NBP2-44751), anti–pan-laminin (Millipore AB2034), anti–Ki-67–FITC (eBioscience 11-5698-80), anti-ABCA3 (Seven Hills WMAB-13H257), and anti–phospho-p65 (S276) (Abcam ab106129). The following secondary antibodies were used: anti-rabbit Alexa Fluor 488 (Life Technologies A21206), anti-rabbit Alexa Fluor 594 (Life Technologies A21207), anti-mouse Alexa Fluor 488 (Life Technologies A11001), and anti-rat Alexa Flour 488 (Life Technologies A21208). TUNEL staining was performed per the manufacturer's instructions (Roche 11684795910). Quantification of immunostained sections was performed on 20 nonoverlapping images obtained with a ×20 objective.

TEM. Lungs were harvested from 3-month-old $\beta1^{rtTA}$ and $\beta1^{f/f}$ mice, processed, postfixed with potassium ferrous cyanide, dehydrated with graded acetone, thick sectioned at 1 μm, thin sectioned at 80 nm in the region of interest, and imaged using a Philips FEI T-12 transmission electron microscope in the Vanderbilt Cell Imaging Shared Resource core.

Bronchoalveolar lavage. Sterile saline lavages were performed with 1 mL PBS after sacrifice. Lavage fluid was centrifuged at 270 *g* at 4°C, and cells were resuspended and counted. The Pierce BCA Protein Assay kit (Thermo Fisher Scientific, 23225) was used to test for BALF protein per the manufacturer's instructions. For immunofluorescence analysis of immune cells collected by bronchoalveolar lavage, 40,000 cells were spun onto Shandon cytoslides (Thermo Fisher Scientific) at 240 *g* for 7 minutes, dried, and immunostained per the above protocol.

AEC isolation and collection of conditioned medium. Type 2 AECs were isolated from 3-month-old $\beta1^{rtTA}$ and $\beta1^{f/f}$ mice as previously described, yielding more than 90% type 2 AECs (22, 97, 98). Briefly, a single-cell suspension was generated with a 40-minute dispase digestion and 100-μm, 40-μm, and-20 μm serial filtration. The suspension was then incubated at 37°C for 2 hours in anti-CD45 (BD 553076) and anti- CD32 (BD 553142) antibody–coated plates for negative selection. The medium containing epithelial cells was collected and spun down, and AECs were plated in 5% bronchial epithelial cell growth medium (BEGM) on Matrigel-coated wells with or without the indicated treatment. Treatment reagents included TEMPOL (Sigma-Aldrich 176141) and DPI (Sigma-Aldrich D2926). Medium was collected at 24 hours for analysis.

Western blotting. Protein (60 μg) collected from type 2 AEC isolations was electrophoresed in a 10% gel and transferred onto nitrocellulose membranes. Membranes were blocked, incubated with primary antibody (anti–β_1 integrin [Millipore MAB1997], anti–claudin-3 [Invitrogen 341700], anti-GAPDH [Invitrogen MA5-15738]), and incubated with Odyssey IRDye 800CW and 680RD secondary antibodies. Signal was detected using a LI-COR Odyssey CLx Near-Infrared Western Blot Detection system.

qPCR. RNA was isolated from freshly isolated primary type 2 AECs using the RNEasy Plus Mini Kit (QIAGEN) and cDNA synthesized using the SuperScript VILO Master Mix kit (Thermo Fisher Scientific). qPCR reactions were performed in triplicate using TaqMan PCR Fast Advanced Master Mix (Applied Biosystems, Thermo Fisher Scientific) on a StepOne Plus PCR System (Applied Biosystems) using the following TaqMan probes (Applied Biosystems, Thermo Fischer Scientific): *Claudin-4* Mm00515514_s1, *Claudin-18* Mm00517321_m1, *CD47* Mm00495011_m1, *Duox1* Mm01328685_m1, *Duox2* Mm01326247_m1, *Nox1* Mm00549170_m1, *Nox2* Mm01287743_m1, *Nox4* Mm00479246_m1, and *GAPDH* Mm99999915_g1. Data were normalized to the housekeeping gene *GAPDH*. Relative quantities were analyzed using $\beta1^{f/f}$ values as control.

ELISA and multiplex assay. ELISA for CCL2 and CX3CL1 on AEC conditioned media was performed in triplicate according to the manufacturer's instructions (R&D Systems, MJE00 and MCX310, respectively). Cytokine/chemokine Magnetic Bead 32-Multiplex Panel (Millipore MCYTMAG-70K-PX32) assay was performed on monocyte/macrophage conditioned media, AEC conditioned media, and whole lung tissue lysates in triplicate per the manufacturer's instructions. Tissue lysates were generated by sonicating the right upper lobe, centrifuging the tissue mixture, collecting the supernatant, and normalizing to protein. The Multiplex assay was read on the Luminex MAGPIX platform in the Vanderbilt Hormone and Analytical Services Core.

Flow cytometry. We used collagenase XI (Sigma-Aldrich C7657, 0.7 mg/mL) and type IV DNAse (Sigma-Aldrich D5025, 30 μg/ml) digestion and 40-μm filtration to obtain a single-cell whole lung suspension for flow cytometry analysis. Briefly, cells were blocked with anti-CD32 antibody (BD 553142), incubated with conjugated primary antibody, and analyzed using a 5-laser BD LSR II analytical flow cytometer (BD Biosciences) and FlowJo analysis software (Becton, Dickinson, and Co.). Both single antibody and fluorescence-minus-one controls were used for compensation. The following primary conjugated antibodies were used in flow cytometry experiments: CD45-BV650 (BioLegend 103151), CD64-APC (BioLegend 139306), CD11b–PE-Cy7 (BD 561098), CD11c–PE-Cy5 (eBioscience 15-0114-82), and Ly6C-APC-Cy7 (BD 560596).

Efferocytosis assay. Macrophages collected by bronchoalveolar lavage (5×10^4 cells/well) were plated for 4 hours in serum-free media and exposed to fluorescently labeled primary type 2 AECs (Millipore 382065) from $\beta1^{rtTA}$ mice (1×10^5 cell/well) for 1 hour. After incubation, nonadherent cells were removed by careful washing, and fluorescence was detected on a Molecular Devices SpectraMax M5 Plate Reader.

Macrophage migration assay. Conditioned medium from primary $\beta1^{rtTA}$ and $\beta1^{f/f}$ AECs was placed in the bottom chamber of a 5-μm Transwell insert (Corning 3422). WT macrophages (40,000 per insert) were obtained from pooled BALF and placed in the top chamber, incubated at 37°C for 4 hours. Unmigrated macrophages were removed from the top chamber, while migrated macrophages were fixed to the underside of the Transwell membrane and stained using the spHema 3 Manual Staining System

(protocol 122-911, Fisher Scientific). Five nonoverlapping images of stained migrated macrophages were taken, and the number of migrated cells/field was quantified.

ROS assays. LumiMax Superoxide Anion Detection Kit (Agilent Technologies 204525) was used to detect superoxide from primary type 2 AECs per the manufacturer's instructions. Amplex Red assay (Invitrogen, Thermo Fisher Scientific A22188) was used to detect H_2O_2 released from primary type 2 AECs per the manufacturer's instructions. MitoSOX assay (Thermo Fisher Scientific M36008) was performed on primary type 2 AECs per the manufacturer's instructions. For inhibitor studies, we used TEMPOL (Sigma-Aldrich 176141, 2 mM) and DPI (Sigma-Aldrich D2926, 10 μM).

Statistics. A 2-tailed Student's *t* test was used for comparisons between 2 groups, with results representing mean SEM. For comparisons between 3 or 4 groups, an ordinary 1-way ANOVA was used with secondary analysis by Tukey's test for multiple comparisons as indicated. For both statistical analyses, $P < 0.05$ was considered statistically significant.

Study approval. All animal experiments were approved by the Vanderbilt University Medical Center Institutional Animal Care and Use Committee.

Author contributions

EJP, JTB, JMS, PMG, LAG, SK, SMH, VVP, and WH designed and performed experiments and analyzed data. EJP, TSB, RZ, and LRY conceived the study and designed experiments. EJP, TSB, LRY, RZ, AP, and SHG wrote and edited the manuscript.

Acknowledgments

This work was supported by NIH grants K08 HL127102 (EJP), K08 HL133484 (JTB), R01 DK069921 (RZ), P01 HL092870 (TSB), R01 DK119212 (AP), R01 HL119503 (LRY), R01 GM108807 (SHG), and 5K12HD087023 (JMS); the Francis Family Foundation (JMS); and US Department of Veteran Affairs grants I01 BX002196 (RZ), I01 BX002378 (TSB), and I01 BX002025 (AP). AP is the recipient of a Veterans Affairs Senior Research Career Scientist Award. The authors would like to thank Brittany Matlock, Stephanie Doss, Cathy Alford, Bryan Millis, Riet van der Meer, and Janice Williams for technical assistance. Experiments were performed in part through the use of the Vanderbilt Cell Imaging Shared Resource (supported by NIH grants CA68485, DK20593, DK58404, DK59637, and EY08126). Flow cytometry experiments were performed in the VMC Flow Cytometry Shared Resource. The VMC Flow Cytometry Shared Resource is supported by the Vanderbilt Ingram Cancer Center (P30 CA68485) and the Vanderbilt Digestive Disease Research Center (DK058404).

Address correspondence to: Erin Plosa, 2215B Garland Avenue, 1125 MRB4/Light Hall, Vanderbilt University Medical Center, Nashville, Tennessee 37232, USA. Phone: 615.343.4876; Email: erin.plosa@vumc.org.

1. Hynes RO. Integrins: versatility, modulation, and signaling in cell adhesion. *Cell*. 1992;69(1):11–25.
2. Hynes RO. Integrins: bidirectional, allosteric signaling machines. *Cell*. 2002;110(6):673–687.
3. Humphrey JD, Dufresne ER, Schwartz MA. Mechanotransduction and extracellular matrix homeostasis. *Nat Rev Mol Cell Biol*. 2014;15(12):802–812.
4. Iskratsch T, Wolfenson H, Sheetz MP. Appreciating force and shape — the rise of mechanotransduction in cell biology. *Nat Rev Mol Cell Biol*. 2014;15(12):825–833.
5. Gu BH, Madison MC, Corry D, Kheradmand F. Matrix remodeling in chronic lung diseases. *Matrix Biol*. 2018;73:52–63.
6. Legate KR, Wickström SA, Fässler R. Genetic and cell biological analysis of integrin outside-in signaling. *Genes Dev*. 2009;23(4):397–418.
7. Schwartz MA, Ginsberg MH. Networks and crosstalk: integrin signalling spreads. *Nat Cell Biol*. 2002;4(4):E65–E68.
8. Sun Z, Guo SS, Fässler R. Integrin-mediated mechanotransduction. *J Cell Biol*. 2016;215(4):445–456.
9. Zhou Y, et al. Extracellular matrix in lung development, homeostasis and disease. *Matrix Biol*. 2018;73:77–104.
10. Yazlovitskaya EM, et al. The laminin binding α3 and α6 integrins cooperate to promote epithelial cell adhesion and growth. *Matrix Biol*. 2019;77:101–116.
11. Zhang X, et al. beta1 integrin is necessary for ureteric bud branching morphogenesis and maintenance of collecting duct structural integrity. *Development*. 2009;136(19):3357–3366.
12. Wu W, et al. Beta1-integrin is required for kidney collecting duct morphogenesis and maintenance of renal function. *Am J Physiol Renal Physiol*. 2009;297(1):F210–F217.
13. Kanasaki K, et al. Integrin beta1-mediated matrix assembly and signaling are critical for the normal development and function of the kidney glomerulus. *Dev Biol*. 2008;313(2):584–593.
14. Brakebusch C, et al. Skin and hair follicle integrity is crucially dependent on beta 1 integrin expression on keratinocytes. *EMBO*

J. 2000;19(15):3990–4003.
15. Menko AS, Kreidberg JA, Ryan TT, Van Bockstaele E, Kukuruzinska MA. Loss of alpha3beta1 integrin function results in an altered differentiation program in the mouse submandibular gland. *Dev Dyn*. 2001;220(4):337–349.
16. De Arcangelis A, Mark M, Kreidberg J, Sorokin L, Georges-Labouesse E. Synergistic activities of alpha3 and alpha6 integrins are required during apical ectodermal ridge formation and organogenesis in the mouse. *Development*. 1999;126(17):3957–3968.
17. Jones RG, et al. Conditional deletion of beta1 integrins in the intestinal epithelium causes a loss of Hedgehog expression, intestinal hyperplasia, and early postnatal lethality. *J Cell Biol*. 2006;175(3):505–514.
18. Taddei I, et al. Beta1 integrin deletion from the basal compartment of the mammary epithelium affects stem cells. *Nat Cell Biol*. 2008;10(6):716–722.
19. Li N, et al. Beta1 integrins regulate mammary gland proliferation and maintain the integrity of mammary alveoli. *EMBO J*. 2005;24(11):1942–1953.
20. Naylor MJ, et al. Ablation of beta1 integrin in mammary epithelium reveals a key role for integrin in glandular morphogenesis and differentiation. *J Cell Biol*. 2005;171(4):717–728.
21. Chen J, Krasnow MA. Integrin beta 1 suppresses multilayering of a simple epithelium. *PLoS ONE*. 2012;7(12):e52886.
22. Plosa EJ, et al. Epithelial β1 integrin is required for lung branching morphogenesis and alveolarization. *Development*. 2014;141(24):4751–4762.
23. Pozzi A, Zent R. Extracellular matrix receptors in branched organs. *Curr Opin Cell Biol*. 2011;23(5):547–553.
24. Viquez OM, et al. Integrin alpha6 maintains the structural integrity of the kidney collecting system. *Matrix Biol*. 2017;57-58:244–257.
25. Hyde DM, Tyler NK, Putney LF, Singh P, Gundersen HJ. Total number and mean size of alveoli in mammalian lung estimated using fractionator sampling and unbiased estimates of the Euler characteristic of alveolar openings. *Anat Rec A Discov Mol Cell Evol Biol*. 2004;277(1):216–226.
26. Knust J, Ochs M, Gundersen HJ, Nyengaard JR. Stereological estimates of alveolar number and size and capillary length and surface area in mice lungs. *Anat Rec (Hoboken)*. 2009;292(1):113–122.
27. Weibel ER, Hsia CC, Ochs M. How much is there really? Why stereology is essential in lung morphometry. *J Appl Physiol*. 2007;102(1):459–467.
28. Polverino F, Seys LJ, Bracke KR, Owen CA. B cells in chronic obstructive pulmonary disease: moving to center stage. *Am J Physiol Lung Cell Mol Physiol*. 2016;311(4):L687–L695.
29. Bianchi SM, Dockrell DH, Renshaw SA, Sabroe I, Whyte MK. Granulocyte apoptosis in the pathogenesis and resolution of lung disease. *Clin Sci*. 2006;110(3):293–304.
30. Hodge S, Hodge G, Holmes M, Reynolds PN. Increased airway epithelial and T-cell apoptosis in COPD remains despite smoking cessation. *Eur Respir J*. 2005;25(3):447–454.
31. Rock JR, et al. Multiple stromal populations contribute to pulmonary fibrosis without evidence for epithelial to mesenchymal transition. *Proc Natl Acad Sci U S A*. 2011;108(52):E1475–E1483.
32. Desai TJ, Brownfield DG, Krasnow MA. Alveolar progenitor and stem cells in lung development, renewal and cancer. *Nature*. 2014;507(7491):190–194.
33. Barkauskas CE, et al. Type 2 alveolar cells are stem cells in adult lung. *J Clin Invest*. 2013;123(7):3025–3036.
34. Hogan BL, et al. Repair and regeneration of the respiratory system: complexity, plasticity, and mechanisms of lung stem cell function. *Cell Stem Cell*. 2014;15(2):123–138.
35. Hewlett JC, Kropski JA, Blackwell TS. Idiopathic pulmonary fibrosis: epithelial-mesenchymal interactions and emerging therapeutic targets. *Matrix Biol*. 2018;71-72:112–127.
36. Jones CV, et al. M2 macrophage polarisation is associated with alveolar formation during postnatal lung development. *Respir Res*. 2013;14:41.
37. Lee YJ, et al. Preventing cleavage of Mer promotes efferocytosis and suppresses acute lung injury in bleomycin treated mice. *Toxicol Appl Pharmacol*. 2012;263(1):61–72.
38. McCubbrey AL, Curtis JL. Efferocytosis and lung disease. *Chest*. 2013;143(6):1750–1757.
39. Parks BW, et al. CD36, but not G2A, modulates efferocytosis, inflammation, and fibrosis following bleomycin-induced lung injury. *J Lipid Res*. 2013;54(4):1114–1123.
40. Truman LA, et al. CX3CL1/fractalkine is released from apoptotic lymphocytes to stimulate macrophage chemotaxis. *Blood*. 2008;112(13):5026–5036.
41. Ravichandran KS. Find-me and eat-me signals in apoptotic cell clearance: progress and conundrums. *J Exp Med*. 2010;207(9):1807–1817.
42. Gardai SJ, et al. Cell-surface calreticulin initiates clearance of viable or apoptotic cells through trans-activation of LRP on the phagocyte. *Cell*. 2005;123(2):321–334.
43. Richmond BW, et al. Bacterial-derived neutrophilic inflammation drives lung remodeling in a mouse model of chronic obstructive pulmonary disease. *Am J Respir Cell Mol Biol*. 2018;58(6):736–744.
44. Misharin AV, Morales-Nebreda L, Mutlu GM, Budinger GR, Perlman H. Flow cytometric analysis of macrophages and dendritic cell subsets in the mouse lung. *Am J Respir Cell Mol Biol*. 2013;49(4):503–510.
45. Benjamin JT, et al. Epithelial-derived inflammation disrupts elastin assembly and alters saccular stage lung development. *Am J Pathol*. 2016;186(7):1786–1800.
46. Chen X, et al. Lack of integrin alpha1beta1 leads to severe glomerulosclerosis after glomerular injury. *Am J Pathol*. 2004;165(2):617–630.
47. Chen X, et al. Integrin alpha1beta1 controls reactive oxygen species synthesis by negatively regulating epidermal growth factor receptor-mediated Rac activation. *Mol Cell Biol*. 2007;27(9):3313–3326.
48. Borza CM, et al. Inhibition of integrin α2β1 ameliorates glomerular injury. *J Am Soc Nephrol*. 2012;23(6):1027–1038.
49. Honoré S, Kovacic H, Pichard V, Briand C, Rognoni JB. Alpha2beta1-integrin signaling by itself controls G1/S transition in a human adenocarcinoma cell line (Caco-2): implication of NADPH oxidase-dependent production of ROS. *Exp Cell Res*. 2003;285(1):59–71.

50. Wang H, et al. p47(phox) contributes to albuminuria and kidney fibrosis in mice. *Kidney Int*. 2015;87(5):948–962.
51. Boekhoudt GH, Guo Z, Beresford GW, Boss JM. Communication between NF-kappa B and Sp1 controls histone acetylation within the proximal promoter of the monocyte chemoattractant protein 1 gene. *J Immunol*. 2003;170(8):4139–4147.
52. Martin T, Cardarelli PM, Parry GC, Felts KA, Cobb RR. Cytokine induction of monocyte chemoattractant protein-1 gene expression in human endothelial cells depends on the cooperative action of NF-kappa B and AP-1. *Eur J Immunol*. 1997;27(5):1091–1097.
53. Ping D, Boekhoudt GH, Rogers EM, Boss JM. Nuclear factor-kappa B p65 mediates the assembly and activation of the TNF-responsive element of the murine monocyte chemoattractant-1 gene. *J Immunol*. 1999;162(2):727–734.
54. Abboud RT, Vimalanathan S. Pathogenesis of COPD. Part I. The role of protease-antiprotease imbalance in emphysema. *Int J Tuberc Lung Dis*. 2008;12(4):361–367.
55. Hendrix AY, Kheradmand F. The role of matrix metalloproteinases in development, repair, and destruction of the lungs. *Prog Mol Biol Transl Sci*. 2017;148:1–29.
56. Janoff A, et al. Experimental emphysema induced with purified human neutrophil elastase: tissue localization of the instilled protease. *Am Rev Respir Dis*. 1977;115(3):461–478.
57. Cheng DS, et al. Airway epithelium controls lung inflammation and injury through the NF-kappa B pathway. *J Immunol*. 2007;178(10):6504–6513.
58. Zaynagetdinov R, et al. Chronic NF-κB activation links COPD and lung cancer through generation of an immunosuppressive microenvironment in the lungs. *Oncotarget*. 2016;7(5):5470–5482.
59. Kim C, et al. Attenuation of cigarette smoke-induced emphysema in mice by apolipoprotein A-1 overexpression. *Am J Respir Cell Mol Biol*. 2016;54(1):91–102.
60. Tuder RM, Petrache I, Elias JA, Voelkel NF, Henson PM. Apoptosis and emphysema: the missing link. *Am J Respir Cell Mol Biol*. 2003;28(5):551–554.
61. Aoshiba K, Yokohori N, Nagai A. Alveolar wall apoptosis causes lung destruction and emphysematous changes. *Am J Respir Cell Mol Biol*. 2003;28(5):555–562.
62. Kasahara Y, et al. Inhibition of VEGF receptors causes lung cell apoptosis and emphysema. *J Clin Invest*. 2000;106(11):1311–1319.
63. Yoshida S, et al. Annexin V decreases PS-mediated macrophage efferocytosis and deteriorates elastase-induced pulmonary emphysema in mice. *Am J Physiol Lung Cell Mol Physiol*. 2012;303(10):L852–L860.
64. Wang X, et al. Dysregulation of TGF-beta1 receptor activation leads to abnormal lung development and emphysema-like phenotype in core fucose-deficient mice. *Proc Natl Acad Sci U S A*. 2005;102(44):15791–15796.
65. Zhao Y, et al. Deletion of core fucosylation on alpha3beta1 integrin down-regulates its functions. *J Biol Chem*. 2006;281(50):38343–38350.
66. Nakamura T, et al. Fibulin-5/DANCE is essential for elastogenesis in vivo. *Nature*. 2002;415(6868):171–175.
67. Nakamura T. Roles of short fibulins, a family of matricellular proteins, in lung matrix assembly and disease. *Matrix Biol*. 2018;73:21–33.
68. Janssen-Heininger YM, et al. Nuclear factor kappaB, airway epithelium, and asthma: avenues for redox control. *Proc Am Thorac Soc*. 2009;6(3):249–255.
69. Pantano C, Reynaert NL, van der Vliet A, Janssen-Heininger YM. Redox-sensitive kinases of the nuclear factor-kappaB signaling pathway. *Antioxid Redox Signal*. 2006;8(9-10):1791–1806.
70. Moodie FM, et al. Oxidative stress and cigarette smoke alter chromatin remodeling but differentially regulate NF-kappaB activation and proinflammatory cytokine release in alveolar epithelial cells. *FASEB J*. 2004;18(15):1897–1899.
71. Sheng ZG, Huang W, Liu YX, Yuan Y, Zhu BZ. Ofloxacin induces apoptosis via β1 integrin-EGFR-Rac1-Nox2 pathway in microencapsulated chondrocytes. *Toxicol Appl Pharmacol*. 2013;267(1):74–87.
72. Chen X, et al. Integrin alpha1beta1 regulates epidermal growth factor receptor activation by controlling peroxisome proliferator-activated receptor gamma-dependent caveolin-1 expression. *Mol Cell Biol*. 2010;30(12):3048–3058.
73. Blackwell TS, et al. NF-κB signaling in fetal lung macrophages disrupts airway morphogenesis. *J Immunol*. 2011;187(5):2740–2747.
74. Henson PM, Hume DA. Apoptotic cell removal in development and tissue homeostasis. *Trends Immunol*. 2006;27(5):244–250.
75. Kresch MJ, Christian C, Wu F, Hussain N. Ontogeny of apoptosis during lung development. *Pediatr Res*. 1998;43(3):426–431.
76. Winter C, et al. Important role for CC chemokine ligand 2-dependent lung mononuclear phagocyte recruitment to inhibit sepsis in mice infected with Streptococcus pneumoniae. *J Immunol*. 2009;182(8):4931–4937.
77. Boniakowski AE, et al. Murine macrophage chemokine receptor CCR2 plays a crucial role in macrophage recruitment and regulated inflammation in wound healing. *Eur J Immunol*. 2018;48(9):1445–1455.
78. Larson SR, et al. Ly6C(+) monocyte efferocytosis and cross-presentation of cell-associated antigens. *Cell Death Differ*. 2016;23(6):997–1003.
79. Serhan CN, Savill J. Resolution of inflammation: the beginning programs the end. *Nat Immunol*. 2005;6(12):1191–1197.
80. Morimoto K, Janssen WJ, Terada M. Defective efferocytosis by alveolar macrophages in IPF patients. *Respir Med*. 2012;106(12):1800–1803.
81. Vandivier RW, et al. Impaired clearance of apoptotic cells from cystic fibrosis airways. *Chest*. 2002;121(3 suppl):89S.
82. Vandivier RW, Henson PM, Douglas IS. Burying the dead: the impact of failed apoptotic cell removal (efferocytosis) on chronic inflammatory lung disease. *Chest*. 2006;129(6):1673–1682.
83. Vandivier RW, et al. Dysfunctional cystic fibrosis transmembrane conductance regulator inhibits phagocytosis of apoptotic cells with proinflammatory consequences. *Am J Physiol Lung Cell Mol Physiol*. 2009;297(4):L677–L686.
84. Huynh ML, et al. Defective apoptotic cell phagocytosis attenuates prostaglandin E2 and 15-hydroxyeicosatetraenoic acid in severe asthma alveolar macrophages. *Am J Respir Crit Care Med*. 2005;172(8):972–979.
85. Hodge S, Hodge G, Scicchitano R, Reynolds PN, Holmes M. Alveolar macrophages from subjects with chronic obstructive pulmonary disease are deficient in their ability to phagocytose apoptotic airway epithelial cells. *Immunol Cell Biol*. 2003;81(4):289–296.
86. Kirkham PA, Spooner G, Rahman I, Rossi AG. Macrophage phagocytosis of apoptotic neutrophils is compromised by matrix proteins modified by cigarette smoke and lipid peroxidation products. *Biochem Biophys Res Commun*. 2004;318(1):32–37.
87. Elias BC, et al. The integrin β1 subunit regulates paracellular permeability of kidney proximal tubule cells. *J Biol Chem*.

2014;289(12):8532–8544.
88. Kage H, et al. Claudin 4 knockout mice: normal physiological phenotype with increased susceptibility to lung injury. *Am J Physiol Lung Cell Mol Physiol*. 2014;307(7):L524–L536.
89. Li G, et al. Knockout mice reveal key roles for claudin 18 in alveolar barrier properties and fluid homeostasis. *Am J Respir Cell Mol Biol*. 2014;51(2):210–222.
90. Zhou B, et al. Claudin-18-mediated YAP activity regulates lung stem and progenitor cell homeostasis and tumorigenesis. *J Clin Invest*. 2018;128(3):970–984.
91. LaFemina MJ, et al. Claudin-18 deficiency results in alveolar barrier dysfunction and impaired alveologenesis in mice. *Am J Respir Cell Mol Biol*. 2014;51(4):550–558.
92. Kim KA, Jung JH, Kang IG, Choi YS, Kim ST. ROS is involved in disruption of tight junctions of human nasal epithelial cells induced by HRV16. *Laryngoscope*. 2018;128(12):E393–E401.
93. Yu L, Gan X, Liu X, An R. Calcium oxalate crystals induces tight junction disruption in distal renal tubular epithelial cells by activating ROS/Akt/p38 MAPK signaling pathway. *Ren Fail*. 2017;39(1):440–451.
94. Gangwar R, et al. Calcium-mediated oxidative stress: a common mechanism in tight junction disruption by different types of cellular stress. *Biochem J*. 2017;474(5):731–749.
95. Perl AK, Tichelaar JW, Whitsett JA. Conditional gene expression in the respiratory epithelium of the mouse. *Transgenic Res*. 2002;11(1):21–29.
96. Raghavan S, Bauer C, Mundschau G, Li Q, Fuchs E. Conditional ablation of beta1 integrin in skin. Severe defects in epidermal proliferation, basement membrane formation, and hair follicle invagination. *J Cell Biol*. 2000;150(5):1149–1160.
97. Rice WR, Conkright JJ, Na CL, Ikegami M, Shannon JM, Weaver TE. Maintenance of the mouse type II cell phenotype in vitro. *Am J Physiol Lung Cell Mol Physiol*. 2002;283(2):L256–L264.
98. Young LR, et al. The alveolar epithelium determines susceptibility to lung fibrosis in Hermansky-Pudlak syndrome. *Am J Respir Crit Care Med*. 2012;186(10):1014–1024.